ACS OMEGA

Open Access

This article is licensed under CC-BY-NC-ND 4.0

http://pubs.acs.org/journal/acsodf

Article

Targeted Therapy with Cisplatin-Loaded Calcium Citrate Nanoparticles Conjugated with Epidermal Growth Factor for Lung Cancer Treatment

Lipika Oopkaew, Yuwanda Injongkol, Natchanon Rimsueb, Panupong Mahalapbutr, Kiattawee Choowongkomon, Sarinya Hadsadee, Rojrit Rojanathanes,* and Thanyada Rungrotmongkol*

Cite This: *ACS Omega* 2024, 9, 25668−25677

Read Online

ACCESS | Metrics & More | Article Recommendations | Supporting Information

ABSTRACT: Lung cancer is the leading cause of cancer-related deaths worldwide with high incidence rates for new cases. Conventional cisplatin (CDDP) therapy has limitations due to severe side effects from nonspecific targeting. To address this challenge, nanomedicine offers targeted therapies. In this study, cisplatin-loaded calcium citrate nanoparticles conjugated with epidermal growth factor (CaCit@CDDP-EGF NPs) were synthesized. The resulting nanodrug had a size below 350 nm with a cation charge. Based on density functional theory (DFT), the CaCit@CDDP NP model containing two citrates substituted on two chlorides exhibited a favorable binding energy of −5.42 eV, and the calculated spectrum at 261 nm closely matched the experimental data. CaCit@CDDP-EGF NPs showed higher inhibition rates against EGFR-expressed and mutant carcinoma cells compared to those of cisplatin while displaying lower cytotoxicity to lung fibroblast cells. Integrating *in vitro* experiments with *in silico* studies, these nanoparticles hold promise as a novel nanomedicine for targeted therapy in clinical applications.

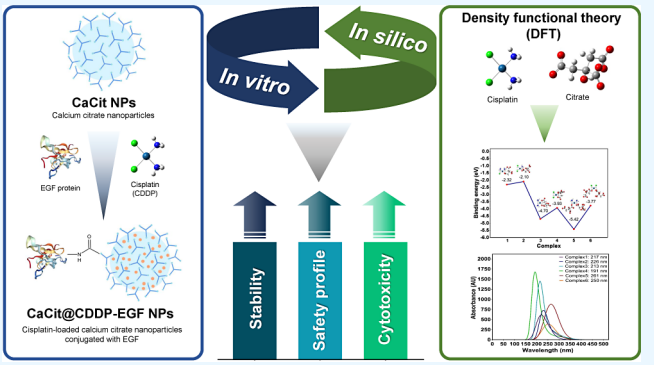

1. INTRODUCTION

According to the International Agency for Research on Cancer (IARC) 2020 report on global cancer statistics, the incidence and mortality rates of cancer are projected to rise continuously. Among various cancer types, lung cancer, specifically bronchogenic carcinoma, stands as the leading cause of cancer-related deaths, accounting for approximately 1.8 million fatalities (18% of the total) and ranking as the second most commonly diagnosed cancer worldwide with an estimated 11.4% of new cases.[1] Nonsmall cell lung cancer (NSCLC) represents around 85% of lung cancer cases, while small cell lung cancer (SCLC) accounts for the remaining 15%. Current therapeutic approaches for both types include surgery, radiation therapy, photodynamic therapy, and chemotherapy, which exhibit effectiveness primarily in noninvasive cases but still pose a risk of recurrence.[2−4] Notably, the use of cisplatin is a cornerstone in cancer treatment; however, there are limitations such as oral drug degradation *in vitro* due to sensitivity to chemical reactions[5,6] and severe clinical side effects including nausea, nephrotoxicity, and hepatotoxicity resulting from the lack of specific targeting sites through intravenous administration.[7,8] Cisplatin (CDDP), also known as *cis*-diamminedichloroplatinum(II), is an FDA-approved platinum-based drug. Its mechanism of action involves inhibiting cell growth by binding to purine bases, specifically guanine (G) and adenine (A), at the N7 binding site, resulting in DNA damage and structural alterations. This property of cisplatin is responsible for its high cytotoxicity in normal cells, leading to undesirable side effects.[9,10] Density functional theory (DFT) enables the study of molecular structures, binding affinities, and UV−vis spectra. In an effort to gain insights into the mechanism of cisplatin and to mitigate its side effects during therapeutic interventions, the DFT study serves as a valuable approach.[11]

Nanobiomedical technology has emerged as a promising avenue for targeted therapy by enhancing drug stability and delivery and reducing cytotoxicity. Nanosized drug carriers ranging from 100 to 1000 nm have demonstrated the ability to efficiently transport both hydrophobic and hydrophilic molecules.[12] To address the issue of broad size distribution, which can impact drug efficacy and shelf life, the synthesis of calcium citrate nanoparticles (CaCit NPs) was employed to

Received: November 10, 2023
Revised: May 19, 2024
Accepted: May 24, 2024
Published: June 9, 2024

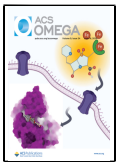

© 2024 The Authors. Published by American Chemical Society

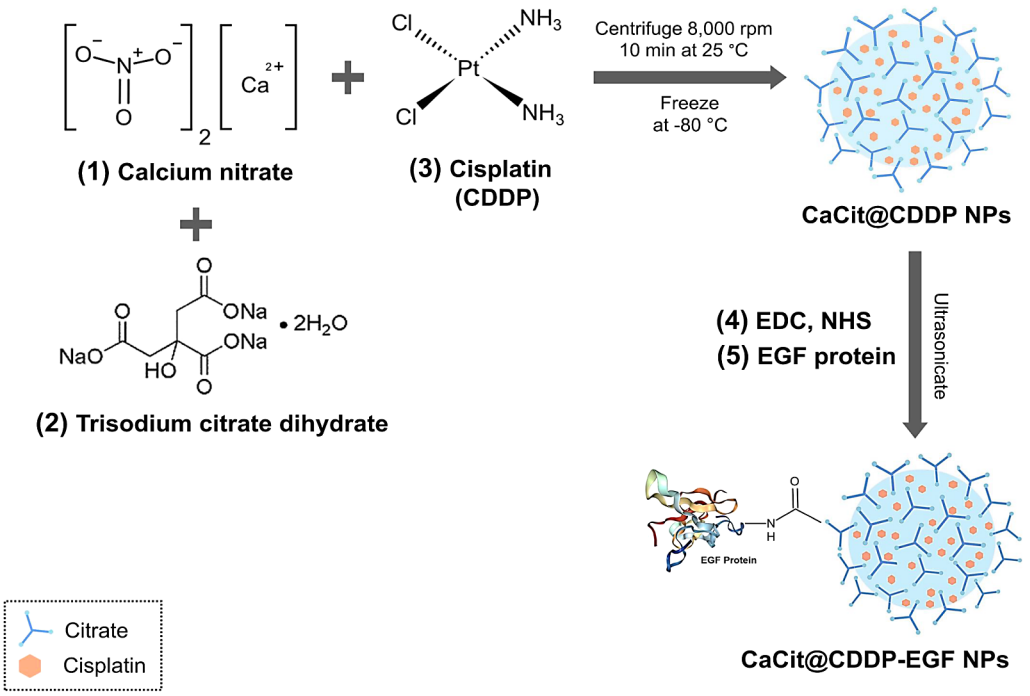

Figure 1. The schematic representation of the synthesis process for calcium citrate nanoparticles conjugated with cisplatin and epidermal growth factor protein (CaCit@CDDP-EGF NPs). Nanoparticles were synthesized by a bottom-up process with the double coprecipitation method.

overcome variations in particle size commonly observed in crystalline polymorphs such as calcium carbonate and other calcium salt particles.[13,14] The potential of CaCit NPs as a carrier for nanodrugs was demonstrated through the synthesis of calcium citrate-based fluorescein isothiocyanate nanoparticles (CaCit-FITC NPs). The synthesis of cisplatin-loaded calcium citrate nanoparticles conjugated with epidermal growth factor (CaCit@CDDP-EGF NPs) was achieved through a coprecipitation method involving calcium and citrate ions in a bottom-up process, enabling control over the cisplatin loading capacity.[15]

The epidermal growth factor receptor (EGFR) is predominantly expressed in carcinoma cells and plays a crucial role in activating tyrosine kinase activity, which regulates cell proliferation and apoptosis. EGF is presented as a commonly detected binding specific ligand in humans with good binding affinity through the size of the molecule around 6.1 kDa.[16,17] The use of EGF as a ligand for EGFR-targeted hollow mesoporous silica nanoparticles (HMSNs) resulted in distinct morphology, X-ray diffraction (XRD) patterns compared to nontargeted nanoparticles, and cellular uptake potential by the active conformation of EGF.[18] These findings highlight the suitability of the EGF protein as a targeting molecule aimed at achieving targeted therapy.

The present study focuses on the development of a targeted nanomedicine for lung cancer therapy utilizing CaCit@CDDP-EGF NPs.[19,20] UV−vis spectrum and DFT calculations were employed to investigate the stability of the nanodrug by studying the binding affinity of CDDP-citrate complexes. We aim to pave the way for future clinical applications.

2. RESULTS

2.1. Synthesis and Characterization of Nanoparticles.

The synthetic pathway for the production of CaCit@CDDP-EGF NPs is shown in Figure 1. The nanoparticles were synthesized by using a bottom-up approach through a double coprecipitation method.

In the present study, different ratios of calcium and citrate ions (Ca^{2+}:$C_6H_5O_7^{3-}$) were utilized (Table S1), with a fixed citrate ratio of 1.0 mM. Hydrodynamic size and zeta potential were measured using DLS, while morphology was observed using SEM. Physical characterization and optimization of the ion reaction ratios are depicted in Figures 2A and 3.

At a reaction ratio of 1.0:1.0 mM Ca^{2+}:$C_6H_5O_7^{3-}$, CaCit NPs were initially formed with sizes smaller than 100 nm (83.54 ± 4.96 nm), exhibiting a needlelike shape (Figure 3A). At the ratio of 1.3:1.0 mM, the sizes ranged from 100 to 150 nm (125.40 ± 5.94 nm) and the particles appeared spherical in shape (Figure 3B). For the reaction ratio of 1.5:1.0 mM, the sizes exceeded 300 nm (376.65 ± 4.70 nm), while at the ratio of 1.6:1.0 mM, the sizes surpassed 500 nm (683.72 ± 8.23 nm). Nanoparticles formed at both of these reaction ratios exhibited needlelike crystal morphology (Figure 3C,D). The polydispersity index (PDI) ranged from 0.102 to 0.182.

Furthermore, the concentrations of calcium and citrate ions were optimized according to Table S2. The results indicate the formation of CaCit NPs with sizes ranging from 100 to 150 nm (135.67 ± 9.26 nm) and a PDI of 0.092 at a concentration of Ca^{2+}:$C_6H_5O_7^{3-}$ of 1.50:1.125 mM. When the concentration was increased to 1.625:1.25 mM, the nanoparticle sizes decreased to below 100 nm (89.36 ± 6.31 nm). Conversely, at lower concentrations (0.75:0.56 mM and 0.38:0.28 mM), the nanoparticle sizes exceeded 200 nm (233.56 ± 7.80 nm for 0.75:0.56 mM and 435.67 ± 6.20 nm for 0.38:0.28 mM). The PDI of the particles showed insignificant changes between the lowest and highest concentrations, ranging from 0.079 to 0.184. The hydrodynamic size and PDI of the particles, which exhibited a concentration-dependent behavior, are depicted in Figure 2B. The morphology of CaCit NPs is illustrated in Figure 4A.

https://doi.org/10.1021/acsomega.3c08969
ACS Omega 2024, 9, 25668−25677

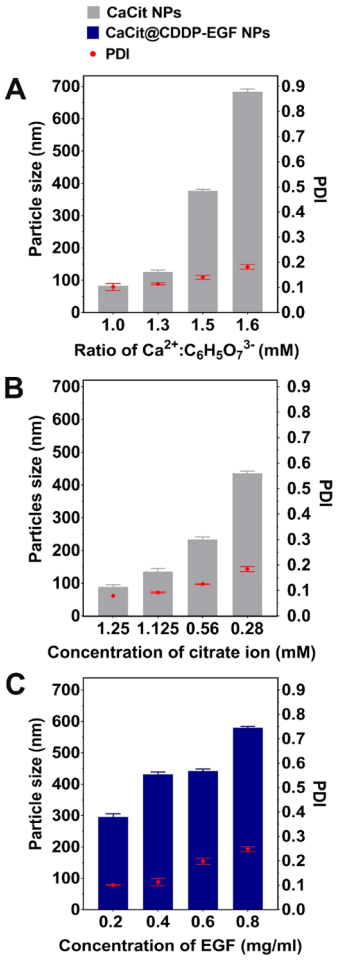

Figure 2. Characterization of nanoparticles and optimization of synthesis conditions. The hydrodynamic sizes were determined using DLS (n = 3, mean ± SD). (A) Hydrodynamic size and PDI of CaCit NPs at different reaction ratios (Ca^{2+}:$C_6H_5O_7^{3-}$) while the citrate ion concentration was fixed at 1.0 mM. (B) Hydrodynamic size and PDI of CaCit NPs at different concentrations of Ca^{2+}:$C_6H_5O_7^{3-}$ ions. (C) Hydrodynamic size and PDI of CaCit@CDDP-EGF NPs at different concentrations of EGF protein conjugated to the nanoparticles.

To incorporate CDDP into the nanoparticles, 20 mg of CDDP was loaded into the solution. Figure 4B illustrates the spherical shape of the CaCit@CDDP NPs, which exhibit larger sizes compared to CaCit NPs (without CDDP).

For the synthesis of CaCit@CDDP-EGF NPs, EGF proteins were employed at various concentrations (0.2, 0.4, 0.6, and 0.8 mg/mL) and conjugated with CaCit@CDDP NPs (Figure 2C). At an EGF concentration of 0.2 mg/mL, CaCit@CDDP-EGF NPs were formed with sizes ranging from 250 to 350 nm (295.63 ± 9.80 nm). SEM imaging revealed a flaky shape with EGF proteins conjugated to the particles (Figure 4C,D). The sizes of the nanoparticles increased with higher concentrations of EGF. For EGF concentrations exceeding 0.2 mg/mL, the particle sizes were larger than 300 nm. The PDI ranged from 0.101 to 0.248.

Figure 4E,F presents the variations in particle sizes and zeta potentials among CaCit NPs, CaCit@CDDP NPs, and CaCit@CDDP-EGF NPs. The hydrodynamic sizes of CaCit NPs (135.13 ± 7.35 nm) and CaCit@CDDP NPs (154.00 ± 10.63 nm) did not exhibit a significant difference. However, following EGF conjugation, the hydrodynamic sizes of CaCit@CDDP-EGF NPs (320.90 ± 23.20 nm) increased significantly (**p = 0.003) compared to CaCit@CDDP NPs (Figure 4E).

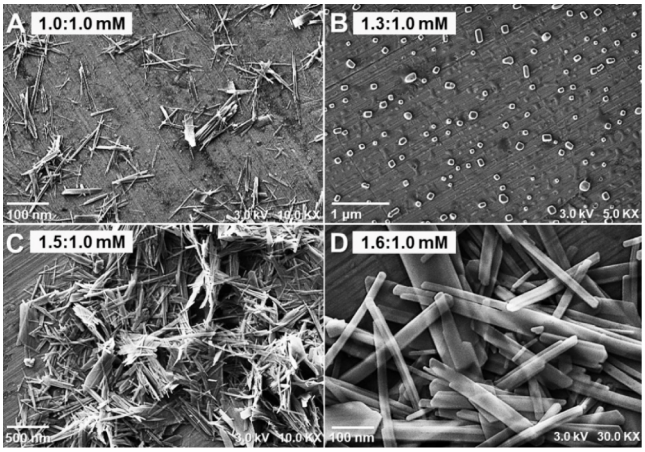

Figure 3. Scanning electron microscope (SEM) images of CaCit NPs at various reaction ratios of Ca^{2+}:$C_6H_5O_7^{3-}$. (A) At 1.0:1.0 mM, particles exhibited a small needlelike shape. (B) At 1.3:1.0 mM, particles displayed a spherical shape. (C and D) At 1.5:1.0 and 1.6:1.0 mM, particles appeared as needlelike crystals with a tendency toward aggregation.

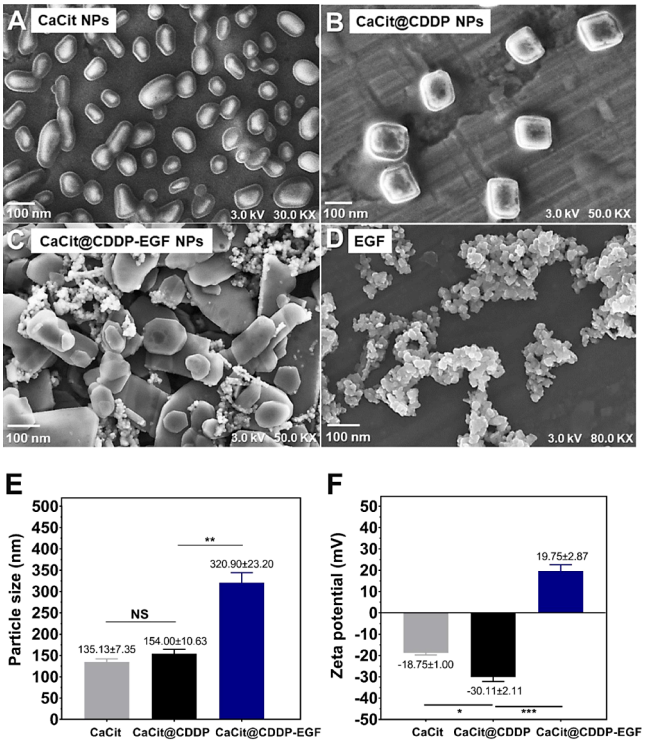

Figure 4. Size and morphology of nanoparticles. (A) Scanning electron microscope (SEM) images of CaCit NPs illustrated as a spherical shape with the size of 100−150 nm, (B) CaCit@CDDP NPs illustrated as a spherical shape with the size of 150−200 nm, and (C) CaCit@CDDP-EGF NPs illustrated as a flakey shape with the size of 250−350 nm. (D) EGF as targeting molecules was detected as globular with a size of 100−500 nm before conjugated with nanoparticles. (E) The hydrodynamic size and (F) zeta potential of nanoparticles from three independent experiments for each particle (n = 3, mean ± SD, * $p \leq 0.05$, ** $p \leq 0.01$, and *** $p \leq 0.001$ versus CaCit@CDDP NPs). NS = no significant difference in statistic analysis.

https://doi.org/10.1021/acsomega.3c08969
ACS Omega 2024, 9, 25668−25677

The zeta charges of CaCit NPs (−18.75 ± 1.00 mV) and CaCit@CDDP NPs (−30.11 ± 2.11 mV) were both anionic and showed no significant difference (*p = 0.018). Upon conjugation with EGF, the zeta charge of CaCit@CDDP-EGF NPs changed from anionic to cationic (+19.75 ± 2.87 mV), which was significantly different (***p = 0.0005) from that of CaCit@CDDP NPs (Figure 4F).

The CDDP content in CaCit@CDDP-EGF NPs was determined by using ICP-AES. A sample containing 600 mg of CaCit@CDDP-EGF NPs was dissolved in 50% DMSO and quantified by comparison to a calibration curve. The loading efficiency of CDDP was calculated to be 62%, resulting in 12.4 mg of cisplatin in 600 mg of particles.

CaCit@CDDP-EGF NPs were stored at −20 °C before freeze-drying, and their stability was evaluated by measuring the hydrodynamic sizes and zeta potentials using DLS over a period of 30 days. No significant differences were observed in the sizes and zeta potentials of the particles. The sizes of CaCit@CDDP-EGF NPs ranged from 301.38 ± 5.59 nm to 285.07 ± 5.66 nm, with a PDI of 0.147−0.190 (Figure 5A). The zeta charges of the particles were consistently cationic, with values of +24.02 ± 3.07 mV to +28.46 ± 4.00 mV from day 1 to day 30 (Figure 5B). Furthermore, the IC_{50} values for the cells treated with CaCit@CDDP-EGF NPs, which were stored for 30 days, did not show significant differences compared to those stored for 1 day, across all cell lines (Figure 5C).

2.2. Prediction of CDDP-Citrate Complex in CaCit@CDDP NPs. The configurations of the CDDP-citrate complexes within the CaCit@CDDP NPs were predicted based on the ligand substitution theory of cisplatin and the potential chemical bonding between atoms. Six distinct configurations of CDDP-citrate complexes were proposed, each involving a varying number of citrate groups ($C_6H_5O_7^{3-}$) interacting with the active sites of -Pt in CDDP. These proposed configurations provide potential binding patterns and arrangements of CDDP and citrate molecules within the CaCit@CDDP NPs.

Figures 6A and S1 display the optimized structures and key geometrical parameters of each complex by using DFT calculations. Our results in Figure 6B revealed that complex 5 with two citrates substituted for two chlorides exhibited a strong interaction with the lowest binding energy of −5.42 eV, followed by complex 3 with citrate monosubstituted on two chloride atoms (−4.70 eV) and complex 4 with citrate monosubstitution on two ammonia groups (−3.93 eV). The bond distances of interest within these complexes, specifically the Pt−O distances, were found in a range from 2.05 to 2.09 Å.

TD-DFT calculations were employed to investigate the adsorption spectrum and compare it with experimental data. Figure 6C,D illustrates the UV−vis spectrum plot obtained from both experimental measurements and theoretical calculations. The experimental UV−vis spectrum of CDDP-citrate displayed the average of the highest peak within the 190−450 nm range (Figure 6C). The calculated spectrum of each CDDP-citrate complex ranged from 190 to 300 nm (Figure 6D), with specific peaks observed at 217, 226, 213, 191, 261, and 250 nm for complexes 1 to 6, respectively. This agreement between computational and experimental results further supports the validity of our proposed CaCit@CDDP NPs and provides insights into the absorption characteristics of the different CDDP-citrate complexes.

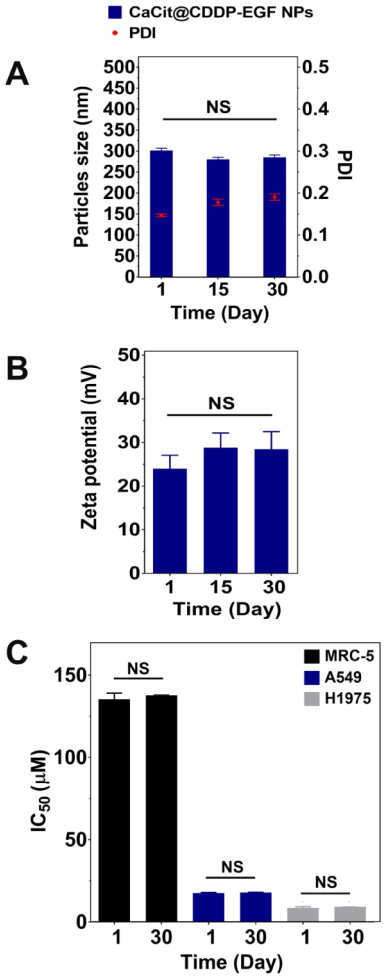

Figure 5. The stability of CaCit@CDDP-EGF NPs during storage for 30 days. (A) The hydrodynamic size with PDI and (B) zeta potentials were determined at 1, 15, and 30 days (n = 3, mean ± SD, * $p \leq 0.05$, ** $p \leq 0.01$, and *** $p \leq 0.001$ versus day 1). (C) IC_{50} values between CaCit@CDDP-EGF NPs stored for over 30 days and day 1, following treatment with MRC-5, A549, and H1975 cell lines (n = 3, mean ± standard error of the mean [SEM], * $p \leq 0.05$, ** $p \leq 0.01$, and *** $p \leq 0.001$ compared to day 1). NS = no significant difference in statistic analysis.

2.3. Effects of CaCit@CDDP-EGF NPs on Cell Viability and Cytotoxicity. The cytotoxicity of CaCit@CDDP-EGF NPs and cisplatin alone was evaluated and is presented in Figure 7A−C. MTT assay was performed on three cell lines, including MRC-5 (normal lung cells), A549 (EGFR-expressing NSCLC cells), and H1975 (mutant EGFR-expressing NSCLC cells). The cell viabilities of MRC-5 and H1975 after treatment with CaCit NPs were above 60%, with no significant difference compared to the control at concentrations below 50 μM. However, in the case of A549 cells, the cell viability was reduced to below 60% compared to the control (****$p \leq$ 0.0001) at concentrations of 25, 50, and 100 μM. The cytotoxic effects on MRC-5 cells were observed when treated with nanoparticles loaded with CDDP. Both CaCit@CDDP NPs and CaCit@CDDP-EGF NPs showed lower cytotoxicity compared to CDDP. The IC_{50} values showed no significant difference between CaCit@CDDP NPs (141.53 ± 6.87 μM) and CaCit@CDDP-EGF NPs (135.36 ± 3.71 μM), but they

https://doi.org/10.1021/acsomega.3c08969
ACS Omega 2024, 9, 25668−25677

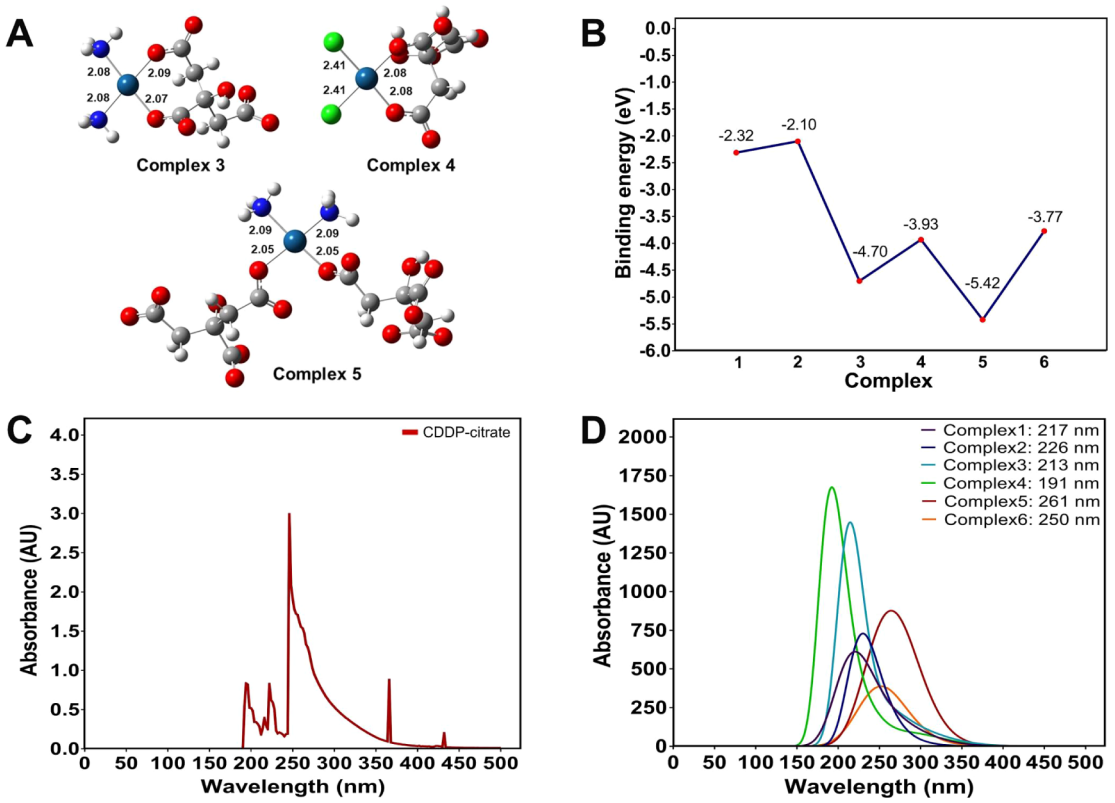

Figure 6. Possible CDDP-citrate complexes, binding energy, and UV−vis spectrum. (A) The optimized CDDP-citrate complexes with favorable binding energy representing the formation of CaCit@CDDP NPs. Additionally, the distances (Å) between -Pt and its ligands are provided for these complexes. Note that the optimized structure of the complexes with unfavorable binding energy is shown in Figure S1. (B) The binding energies (eV) of CDDP-citrate complexes were calculated using DFT at the B3LYP level. (C) The UV−vis spectrum of CDDP-citrate was measured by a spectrophotometer, a spectrum observed in the range of 190−450 nm. (D) The UV−vis spectra of CDDP-citrate complexes obtained from TD-DFT at B3LYP level. Peaks of the theoretical spectra were in the range of 190−300 nm. All computational calculations were computed by the basis set of 6-31G** for nonmetal atoms and LANL2DZ for the metal atom.

were higher (**p = 0.01) compared to CDDP alone (25.37 ± 1.36 μM) (Figure 7D).

To investigate the inhibitory effect, lung cancer cells (A549 and H1975) were treated with cisplatin, CaCit@CDDP NPs, and CaCit@CDDP-EGF NPs. The results revealed concentration-dependent inhibition (Figure 7B,C). When comparing CaCit@CDDP NPs with cisplatin, the IC_{50} values of CaCit@CDDP NPs showed no significant difference from those of CDDP for both A549 and H1975. For A549, the IC_{50} values were 25.57 ± 5.47 μM for CDDP and 37.03 ± 1.45 μM for CaCit@CDDP NPs. For H1975, the IC_{50} values were 41.79 ± 5.57 μM for CDDP and 38.95 ± 4.38 μM for CaCit@CDDP NPs. Comparing CaCit@CDDP NPs with CaCit@CDDP-EGF NPs, the IC_{50} values of CaCit@CDDP-EGF NPs were lower than those of CaCit@CDDP NPs for both A549 and H1975. A549 cells showed an IC_{50} value of 17.61 ± 0.31 μM for CaCit@CDDP-EGF NPs (*p = 0.005), while H1975 cells showed an IC_{50} value of 8.59 ± 0.72 μM (*p = 0.022). When comparing CaCit@CDDP-EGF NPs with CDDP, the IC_{50} value of CaCit@CDDP-EGF NPs for MRC-5 was higher than that of CDDP ($^{\#\#}p$ = 0.004), while H1975 cells showed a lower IC_{50} value than CDDP ($^{\#}p$ = 0.034). The IC_{50} value showed no significant difference from CDDP for A549 (Figure 7E,F).

To study the effect of EGF as a targeting molecule, the cell viability of A549 and H1975 treated with CaCit@CDDP-EGF NPs at a concentration of 0.2 mg/mL decreased in a concentration-dependent manner and significantly decreased (****$p \leq 0.0001$) at a concentration of 100 μM for A549 and a concentration of 50 μM for H1975 compared to CaCit@CDDP NPs. At higher concentrations of EGF (0.4, 0.6, and 0.8 mg/mL), both cell lines showed cell viabilities of up to 60% and significantly higher (****$p \leq 0.0001$) than CaCit@CDDP NPs at concentrations of 12.5 to 100 μM (Figure 8A,B).

3. DISCUSSION

CaCit NPs were selected as CDDP carriers due to their biocompatibility and wide availability in various applications.[13,15] In our study, calcium nitrate and trisodium citrate dihydrate were used as sources of calcium and citrate ions, respectively.[17,18] We achieved the formation of thermodynamically stable CaCit NPs with a needlelike crystal shape at a Ca^{2+}:$C_6H_5O_7^{3-}$ ratio of 1.5:1.0 mM (Figure 3C). The size and shape of the nanoparticles were influenced by the concentration of citrate ions, as reported by Iafisco et al., where citrate played a crucial role in stabilizing the particle's shape and size.[21] Previous studies have also shown that variations in water volume and citrate concentration can result in different nanoparticle shapes, such as tetrahydrate-induced sheet-like structures.[14] This highlights the significance of optimizing the reaction parameters and ion concentrations to control the size and shape of the nanoparticles (Figure 2A,B). The ability to precisely control these factors is crucial for obtaining well-defined nanoparticles with the desired properties and functions.

https://doi.org/10.1021/acsomega.3c08969
ACS Omega 2024, 9, 25668−25677

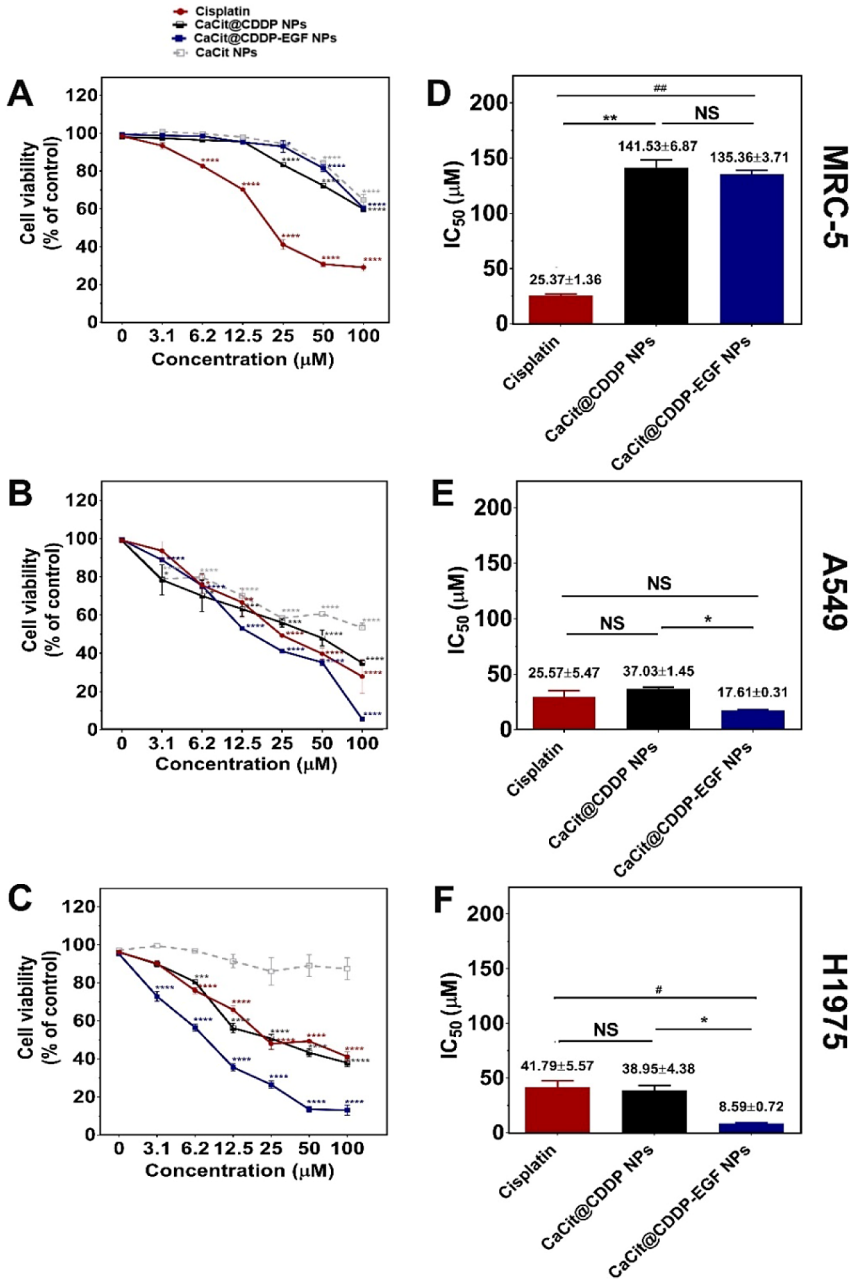

Figure 7. The inhibitory and cytotoxicity effects of CDDP, CaCit NPs, CaCit@CDDP NPs, and CaCit@CDDP-EGF NPs on the lung fibroblast cell line (MRC-5), and lung carcinoma cell lines (A549 and H1975) were determined by MTT assay. (A−C) Percent cell viability of MRC-5, A549, and H1975 was shown as dose-dependent (n = 3, mean ± SEM, Dunnett's multiple comparison tests were performed versus control, * $p \leq 0.05$, ** $p \leq 0.01$, *** $p \leq 0.001$, and **** $p \leq 0.0001$). (D−F) IC_{50} values of MRC-5, A549, and H1975 displayed as mean ± SEM from three independent experiments (n = 3, mean ± SEM, * $p \leq 0.05$, ** $p \leq 0.01$, *** $p \leq 0.001$, and **** $p \leq 0.0001$ versus CaCit@CDDP NPs and $^{\#}$ $p \leq 0.05$, $^{\#\#}$ $p \leq 0.01$, $^{\#\#\#}$ $p \leq 0.001$, and $^{\#\#\#\#}$ $p \leq 0.0001$ versus cisplatin). All statistics were performed using ANOVA with Dunnett's multiple comparison test. NS = no significant difference in statistic analysis.

The size range of 200−500 nm for particles enables uptake through passive and active targeting pathways, providing protection against degradation and a broad distribution.[22] Our study revealed changes in the size, shape, and zeta potential of CaCit NPs, CaCit@CDDP NPs, and CaCit@CDDP-EGF NPs as previously reported.[23] Following CDDP loading and EGF conjugation, particle sizes increased from 100 to 350 nm, while zeta potentials ranged from −30 to +30 mV. The PDI remained below 0.700 (Figure 4E,F). Hydrodynamic size and zeta charges were changed because of EGF targeting and neutralization of negative charges from positive charges of EGF[24] indicating a narrow size distribution and affirming the stability and potential for cellular uptake.[25,26] SEM images depicted the transformation of the particle shape and surface from spherical to flaky with EGF coating (Figure 4A−D).

CDDP in DMSO demonstrated stability for only 8 days, leading to a loss of its inhibitory potency.[27] In terms of nanodrug stability, our findings indicated that CaCit@CDDP-EGF NPs remained stable for 30 days, surpassing the stability of CDDP. Moreover, this extended storage period did not compromise the inhibitory and cytotoxic effects of the nanoparticles (Figure 5). These results underscore the

https://doi.org/10.1021/acsomega.3c08969
ACS Omega 2024, 9, 25668−25677

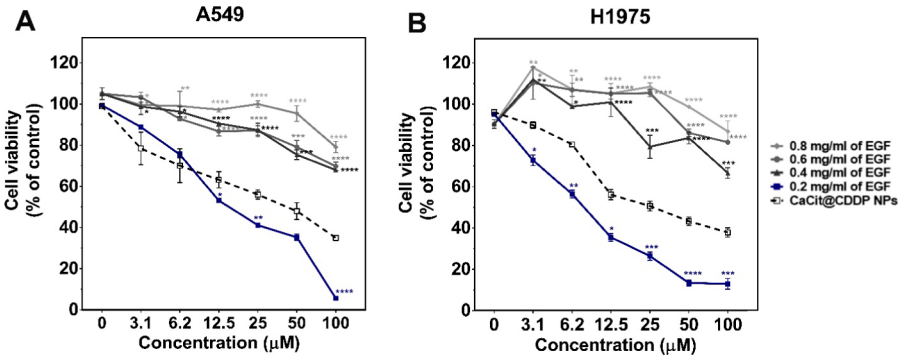

Figure 8. The effect of epidermal growth factor (EGF) protein as a targeting molecule for the inhibition of lung cancer cell lines. The inhibitory effect and cytotoxicity of CaCit@CDDP NPs, and CaCit@CDDP-EGF NPs with EGF 0.2, 0.4, 0.6, and 0.8 mg/mL on (A) EGFR-expressed lung carcinoma cell line (A549) and (B) EGFR mutant-expressed cell line (H1975) were determined by MTT assay (n = 3, mean ± SEM, * $p \leq 0.05$, ** $p \leq 0.01$, *** $p \leq 0.001$, and **** $p \leq 0.0001$ versus CaCit@CDDP NPs). ANOVA with Dunnett's multiple comparison test was used for statistical analysis.

potential of CaCit@CDDP-EGF NPs as a stable and effective nanodrug formulation with an extended shelf life.

DFT calculations were used to study the loading of cisplatin into CaCit NPs, where the ligands comprised chloride (-Cl) atoms and ammonia groups (-NH_3) binding to square planar platinum(II) in the core structure.[11] Among the six possible CDDP-citrate complexes identified (Figure 6A and S1), complexes 3, 4, and 5 exhibited favorable binding energies (Figure 6A,B), making them of particular interest. CDDP's mechanism of action involves the interaction of its -Cl groups with DNA's purine bases, resulting in cancer cell inhibition and high cytotoxicity.[28] Complexes 3 and 5 adhered to the ligand substitution theory, featuring citrate mono- and disubstitution, respectively, on two -Cl atoms. Complex 5, with citrate disubstitution on two -Cl atoms (−5.42 eV), emerged as the most effective complex with a calculated spectrum at 261 nm aligning with the experimental spectrum. Following this, complex 3 with citrate monosubstitution on -Cl atom (−4.70 eV) exhibited a calculated spectrum at 213 nm that correlated with the experimental data. The -NH_3 group in CDDP is considered stable and requires significant energy to dissociate from the core structure within the human body.[29] Complex 4, involving citrate monosubstitution on two -NH_3 molecules, showed a binding energy of −3.93 eV. This suggests that the -NH_3 group may only act as a leaving group in theoretical calculations, as it aligns with the experimental spectrum (191 nm). The *in silico* study suggested the formation of CaCit@CDDP NPs, offering the potential to reduce cytotoxicity by utilizing citrate as a leaving group that binds less tightly to DNA compared to platinum compounds in the traditional mechanism.[30]

CaCit NPs without CDDP loading and EGF conjugation showed minimal cytotoxicity to MRC-5 cells, indicating their biocompatibility. When CDDP was loaded into CaCit NPs, both CaCit@CDDP NPs and CaCit@CDDP-EGF NPs exhibited lower cytotoxicity to MRC-5 cells, with IC_{50} values higher than 100 μM compared to cisplatin. Interestingly, the IC_{50} values of CaCit@CDDP NPs and CaCit@CDDP-EGF NPs were comparable, indicating that the addition of EGF did not significantly alter the cytotoxicity of the nanodrug. However, when comparing CaCit@CDDP NPs and CaCit@CDDP-EGF NPs, the latter showed lower IC_{50} values in A549 and H1975 cells, suggesting enhanced inhibitory effects due to the presence of EGF. These results demonstrate the potential of CaCit@CDDP-EGF NPs as a targeted therapeutic approach for lung cancer.[31]

MTT assay results reported that CaCit@CDDP-EGF NPs had the potential to be a nanocarrier with noncytotoxicity to the lung fibroblast cell line (MRC-5), a normal control cell due to up to 60% viability after treated with CaCit NPs, CaCit@CDDP NPs, and CaCit@CDDP-EGF NPs. Interestingly, lung cancer cell lines (A549 and H1975) were specifically inhibited by CaCit@CDDP-EGF NPs shown with lower IC_{50} values than CDDP (Figure 7). CaCit@CDDP-EGF NPs showed a higher inhibition rate in H1975, which is lung carcinoma with EGFR mutant than wild-type lung carcinoma, A549, due to overexpression of EGFR in H1975.[32] A549 was slightly inhibited by CaCit NPs, described by Jian-Guo Ren and coworkers that citrate suppresses only cancer cells, especially in A549 through the inhibition of multiple mechanisms such as glycolysis and tricarboxylic acid cycle from the study of metabolic profiles.[33]

Our calculation found that complex 5 with two citrate bindings was the most capable and stable complex compared to only one citrate group. This assures the efficiency of our synthesized nanodrug in both *in vitro* and *in silico* studies. Nanoparticles were possibly formed in stable geometries, which decreased cytotoxicity to normal cells.

Additionally, we found that the inhibitory effects were dependent on the EGF amount conjugated with particles in lung carcinoma with the EGFR-expressing cell line (A549) and EGFR mutation cell line (H1975) shown in Figure 8. CaCit@CDDP-EGF NPs with 0.2 mg/mL EGF showed higher inhibition compared with CaCit@CDDP NPs (with no EGF) because of EGF ligand-specific targeting. For CaCit@CDDP-EGF NPs with 0.4 to 0.8 mg/mL of EGF, inhibitory effects were lower than those of CaCit@CDDP NPs due to an excess amount of EGF conjugation which caused size distribution by EGF conformation changing and reduction in EGF−EGFR binding affinity. This can decrease the cellular uptake of A549 and H1975. Therefore, we suggested that optimization of the ligand concentration was important for nanoparticle-targeted ligands. Lower concentrations of EGF showed better inhibition than high concentrations.[18,34]

In conclusion, we found that ion source, reaction ratio, concentration of ions, and amount of targeting molecule could affect the sizes and morphology of synthesized nanodrugs. DFT study confirmed the formation and biological properties

https://doi.org/10.1021/acsomega.3c08969
ACS Omega 2024, 9, 25668−25677

of nanoparticles and provided citrate to be a biocompatible component for nanodrugs. The CaCit@CDDP-EGF NPs have the potential to inhibit lung cancer cells more specifically than commercial CDDP. We successfully found nanomedicine that should be further studied in clinical trials and gives a piece of information and methodology applied to develop metal-based nanoparticle synthesis in future work.

4. METHODS

4.1. Experimental Section. *4.1.1. Chemical Reagents for Nanoparticle Synthesis.* Calcium nitrate (>98.0%) was procured from Carlo Erba (Italy), while trisodium citrate dihydrate (>99.0%) was obtained from Merck (Germany). *cis*-Diamminedichloroplatinum(II), or CDDP, *N*-hydroxysuccinimide (>98.0%), and 1-(3-(dimethylamino)propyl)-3-ethylcarbodiimide (>98.0%) were purchased from Tokyo Chemical Industry (Japan). Epidermal growth factor (EGF) protein was acquired from Sigma-Aldrich (United States). Phosphate-buffered saline (PBS) was sourced from VWR Chemicals (United States).

4.1.2. Synthesis of Calcium Citrate Nanoparticles (CaCit NPs) and Cisplatin-Loaded Calcium Citrate Nanoparticles (CaCit@CDDP NPs). CaCit NPs and CaCit@CDDP NPs were synthesized using a reaction ratio of calcium:citrate ions at 1.3:1.0 mM. The concentrations of calcium and citrate ions were 1.5 and 1.125 mM, respectively. To prepare the stock solutions, 4.92 mg of calcium nitrate and 8.82 mg of trisodium citrate dihydrate were individually dissolved in 10 mL of DI water to achieve a concentration of 3 mM. For the synthesis of CaCit NPs, 2 mL of calcium nitrate, 1.5 mL of trisodium citrate, and 0.5 mL of DI water were combined. For CaCit@CDDP NPs, 0.5 mL of a 20 mg CDDP solution dissolved in 1 mL of 50% DMSO was added instead of DI water. The mixture was stirred on a rocker at room temperature (25 °C) for 2 h for CaCit NPs and 1 h for CaCit@CDDP NPs. Subsequently, the milky suspension was centrifuged at 8000 rpm for 10 min using an Eppendorf 5810R Centrifuge. The resulting white precipitates of nanoparticles were collected, washed five times with DI water, and then frozen and dried at −80 °C to halt the reaction.[15]

4.1.3. Synthesis of Cisplatin-Loaded Calcium Citrate Nanoparticles Conjugated with EGF (CaCit@CDDP-EGF NPs). 800 mg of CaCit@CDDP NPs were dispersed in 1 mL of DI water and subjected to ultrasonication. Following this, 24.5 mg of *N*-hydroxysuccinimide and 0.196 g of 1-(3-(dimethylamino)propyl)-3ethylcarbodiimide were added. An optimized concentration of 0.2 mg/mL of EGF in PBS was introduced into the mixture, along with 2 μL of triethylamine.[18] The mixture was stirred on a rocker for 1 h at room temperature (25 °C) until a homogeneous, milky suspension was obtained. The CaCit@CDDP-EGF NPs were collected by centrifugation at 8000 rpm for 10 min, washed five times with DI water, and then frozen at −80 °C and dried.[15] The synthesized CaCit@CDDP-EGF NPs were stored at −20 °C to stop the reaction. Finally, the nanodrug was freeze-dried by lyophilization and stored for 30 days prior to studying and characterizing stability in physical and biological activities.[35]

4.1.4. Characterization of Nanoparticles. The hydrodynamic size and zeta potential of the nanoparticles were measured using dynamic light scattering (DLS) with a Malvern Zetasizer Nano ZSP. The morphology of the nanoparticles was characterized using a scanning electron microscope (SEM), FESEM (field emission scanning electron microscope), specifically the Carl Zeiss model Auriga. The CDDP content was quantified by inductively coupled plasma atomic emission spectroscopy (ICP-AES) using Thermo Scientific iCAP 6500 instruments. The loading efficiency was calculated using eq 1.[36] Additionally, the UV−vis spectrum of CDDP-citrate was recorded using a spectrophotometer, the Thermo Electron EV 500, in the range of 190−700 nm.

$$\text{Loading efficiency} = \frac{\text{Amount of CDDP in nanoparticles}}{\text{Amount of CDDP loaded to nanoparticles}} \times 100 \quad (1)$$

4.1.5. Cell Culture. Lung fibroblast cells (MRC-5, ATCC−CCL-171) were cultured in Eagle's minimum essential medium (EMEM; Gibco). Lung carcinoma cells (A549, ATCC−CCL-185-LUC2) were cultured in Dulbecco's modified Eagle's medium (DMEM; Gibco). Lung adenocarcinoma cells (H1975, ATCC-CRL-5908) were cultured in Roswell Park Memorial Institute medium (RPMI1640; Gibco). All culture media were supplemented with 10% fetal bovine serum (FBS) and 1% antibiotic−antimycotic. The cell lines were maintained in a humidified atmosphere at 37 °C with 5% CO_2.[37]

4.1.6. Cell Viability Assessment. Cell viability was evaluated using the MTT assay.[38] A549 and H1975 lung cancer cell lines were seeded at a density of 6000 cells/well, while MRC-5 lung fibroblast cells were seeded at 10 000 cells/well in a 96-well plate. All cell lines were seeded in 100 μL of complete culture medium. The plate was then incubated overnight at 37 °C, 5% CO_2 to allow cells to reach 80−90% confluence. For the lung cancer cell lines A549 and H1975, which are EGFR positive, additional treatment with CaCit@CDDP-EGF NPs was performed by using varying concentrations of EGF to assess the effect of EGF concentration as a targeting molecule. CDDP, CaCit NPs, CaCit@CDDP NPs, and CaCit@CDDP-EGF NPs (0.2, 0.4, 0.6, and 0.8 mg/mL of EGF) were dissolved in DMSO at a concentration of 10 mM for stock solutions.[39] The final concentrations were performed by dilution in a complete culture medium. On the next day, the medium was removed and replaced with a complete medium containing varying concentrations of CDDP, CaCit NPs, CaCit@CDDP NPs, and CaCit@CDDP-EGF NPs with 2-fold dilutions, starting at 100 μM (100, 50, 25, 12.5, 6.25, and 3.125 μM). Following treatment, the cells were further incubated for 72 h at 37 °C, 5% CO_2. Subsequently, 10 μL of MTT reagent was added to each well and incubated for an additional 3 h. The culture media were then removed, and 100 μL of dimethyl sulfoxide (DMSO) was added to each well. The plate was stirred on a stirrer for 10 min at room temperature (25 °C) to ensure complete dissolution of formazan crystals. Cell viability was determined by measuring the optical density at 570 nm (OD_{570}). Finally, the half-maximal inhibitory concentration (IC_{50}) values were calculated.[40]

4.1.7. Statistical Analysis. One-way ANOVA with Dunnett's test was performed to compare the cell viability of control with each concentration and the IC_{50} between CDDP and synthesized nanoparticles.[41]

4.2. Computational Section. *4.2.1. Quantum Mechanics (QM) Calculations of CDDP-Citrate Complexes.* The optimized structures of CDDP-citrate NPs were determined by using DFT at the B3LYP level of theory. The 6-31G** basis set was employed for the nonmetal atoms (C, H, N, O, and

https://doi.org/10.1021/acsomega.3c08969
ACS Omega 2024, 9, 25668−25677

Cl), as it has been commonly used in previous studies to investigate the affinity of platinum-based drugs with other molecules, providing valuable information about binding energy and atomic distances between the metal (-Pt) and nonmetal atoms.[11] To accurately describe the -Pt in the core of CDDP, the LANL2DZ basis set was chosen to account for the relativistic effective core potential and ensure appropriate treatment of heavy metal atoms.[42] The conductor-like polarized continuum model (C-PCM) was employed to consider solvent effects on the geometries and absorption spectra. Water was added as the solvent implicitly.[43] This model allowed for the simulation of a solvent environment, enhancing the accuracy of the calculations. The binding energy (EB) was evaluated using eq 2.[44] Additionally, the UV−vis spectrum was computed using time-dependent density functional theory (TD-DFT) at the same level of theory, and the calculated spectrum was compared with experimental data. All calculations were performed using the Gaussian 16 program.[42]

$$EB_{Complex} = E_{Complex} - E_{CDDP} - E_{Citrate} \quad (2)$$

where $E_{Complex}$ represents the total energy of CDDP and citrate. E_{CDDP} and $E_{Citrate}$ represent the total energies of CDDP and citrate, respectively.

■ ASSOCIATED CONTENT

Supporting Information

The Supporting Information is available free of charge at https://pubs.acs.org/doi/10.1021/acsomega.3c08969.

Optimization of conditions for NP synthesis and CDDP-citrate complexes with unfavorable binding energy from computational calculations (PDF)

■ AUTHOR INFORMATION

Corresponding Authors

Rojrit Rojanathanes − *Center of Excellence in Biocatalyst and Sustainable Biotechnology, Department of Chemistry, Faculty of Science, Chulalongkorn University, Bangkok 10330, Thailand*; Phone: +66 22185426; Email: rojrit.r@chula.ac.th

Thanyada Rungrotmongkol − *Center of Excellence in Biocatalyst and Sustainable Biotechnology, Department of Biochemistry, Faculty of Science and Program in Bioinformatics and Computational Biology, Graduate School, Chulalongkorn University, Bangkok 10330, Thailand*; orcid.org/0000-0002-7402-3235; Phone: +66 22185426; Email: Thanyada.r@chula.ac.th

Authors

Lipika Oopkaew − *Center of Excellence in Biocatalyst and Sustainable Biotechnology, Department of Biochemistry, Faculty of Science, Chulalongkorn University, Bangkok 10330, Thailand*

Yuwanda Injongkol − *Center of Excellence in Biocatalyst and Sustainable Biotechnology, Department of Biochemistry, Faculty of Science, Chulalongkorn University, Bangkok 10330, Thailand*

Natchanon Rimsueb − *National Nanotechnology Center NANOTEC, National Science and Technology Development Agency NSTDA, Pathum Thani 12120, Thailand; Center of Excellence in Nanomedicine, Department of Anatomy, Faculty of Medicine, Chulalongkorn University, Bangkok 10330, Thailand*

Panupong Mahalapbutr − *Department of Biochemistry, Center for Translational Medicine, Faculty of Medicine, Khon Kaen University, Khon Kaen 40002, Thailand*; orcid.org/0000-0003-4389-334X

Kiattawee Choowongkomon − *Department of Biochemistry, Faculty of Science, Kasetsart University, Bangkok 10900, Thailand*

Sarinya Hadsadee − *Center of Excellence in Biocatalyst and Sustainable Biotechnology, Department of Biochemistry, Faculty of Science, Chulalongkorn University, Bangkok 10330, Thailand*

Complete contact information is available at: https://pubs.acs.org/10.1021/acsomega.3c08969

Notes

The authors declare no competing financial interest.

■ ACKNOWLEDGMENTS

This research has received funding support from the NSRF via the Program Management Unit for Human Resources & Institutional Development, Research and Innovation (grant number B05F650041). L.O. would like to thank Chulalongkorn University for financing this research as part of the 90th Anniversary of Chulalongkorn University (GCUGR1125651051M) and the Overseas Presentations of Graduate Level Academic Thesis from Graduate School. K.C. gratefully acknowledges the Kasetsart University Research and Development Institute, KURDI (FF(KU)25.644).

■ REFERENCES

(1) Sung, H.; Ferlay, J.; Siegel, R. L.; Laversanne, M.; Soerjomataram, I.; Jemal, A.; Bray, F. Global Cancer Statistics 2020: GLOBOCAN Estimates of Incidence and Mortality Worldwide for 36 Cancers in 185 Countries. *Ca-Cancer J. Clin.* **2021**, *71* (3), 209−249.

(2) Lemjabbar-Alaoui, H.; Hassan, O. U.; Yang, Y. W.; Buchanan, P. Lung cancer: Biology and treatment options. *Biochim. Biophys. Acta* **2015**, *1856* (2), 189−210.

(3) Ji, B.; Wei, M.; Yang, B. Recent advances in nanomedicines for photodynamic therapy (PDT)-driven cancer immunotherapy. *Theranostics* **2022**, *12* (1), 434−458.

(4) Rezakhani, L.; Rashidi, Z.; Mirzapur, P.; Khazaei, M. Antiproliferatory Effects of Crab Shell Extract on Breast Cancer Cell Line (MCF7). *J. Breast Cancer* **2014**, *17* (3), 219−225.

(5) Nakano, K.; Ike, O.; Wada, H.; Hitomi, S.; Amano, Y.; Ogita, I.; Nakai, N.; Takada, K. Oral sustained-release cisplatin preparation for rats and mice. *J. Pharm. Pharmacol.* **2011**, *49* (5), 485−490.

(6) Gavhane, Y. N.; Yadav, A. V. Loss of orally administered drugs in GI tract. *Saudi Pharm. J.* **2012**, *20* (4), 331−344.

(7) Pronk, L. C.; Stoter, G.; Verweij, J. Docetaxel (Taxotere): single agent activity, development of combination treatment and reducing side-effects. *Cancer Treat. Rev.* **1995**, *21* (5), 463−478.

(8) Sanna, V.; Pala, N.; Sechi, M. Targeted therapy using nanotechnology: focus on cancer. *Int. J. Nanomed.* **2014**, *9*, 467−483.

(9) Jamieson, E. R.; Lippard, S. J. Structure, Recognition, and Processing of Cisplatin-DNA Adducts. *Chem. Rev.* **1999**, *99* (9), 2467−2498.

(10) Benhar, M.; Engelberg, D.; Levitzki, A. Cisplatin-induced activation of the EGF receptor. *Oncogene* **2002**, *21* (57), 8723−8731.

(11) Szefler, B.; Czeleń, P.; Krawczyk, P. The Affinity of Carboplatin to B-Vitamins and Nucleobases. *Int. J. Mol. Sci.* **2021**, *22* (7), 3634.

(12) Rizvi, S. A. A.; Saleh, A. M. Applications of nanoparticle systems in drug delivery technology. *Saudi Pharm. J.* **2018**, *26* (1), 64−70.

(13) Akram, M. Citric acid cycle and role of its intermediates in metabolism. *Cell Biochem. Biophys.* **2014**, *68* (3), 475−478.
(14) Li, J.; Liu, Y.; Gao, Y.; Zhong, L.; Zou, Q.; Lai, X. Preparation and properties of calcium citrate nanosheets for bone graft substitute. *Bioengineered* **2016**, *7* (5), 376−381.
(15) Rimsueb, N.; Cherdchom, S.; Aksornkitti, V.; Khotavivattana, T.; Sereemaspun, A.; Rojana Thanes, R. Feeding Cells with a Novel "Trojan" Carrier: Citrate Nanoparticles. *ACS Omega* **2020**, *5* (13), 7418−7423.
(16) Changavi, A. A.; Shashikala, A.; Ramji, A. S. Epidermal Growth Factor Receptor Expression in Triple Negative and Nontriple Negative Breast Carcinomas. *J. Lab. Physicians* **2015**, *7* (2), 79−83.
(17) Byrne, J. D.; Betancourt, T.; Brannon-Peppas, L. Active targeting schemes for nanoparticle systems in cancer therapeutics. *Adv. Drug Delivery Rev.* **2008**, *60* (15), 1615−1626.
(18) She, X.; Chen, L.; Velleman, L.; Li, C.; He, C.; Denman, J.; Wang, T.; Shigdar, S.; Duan, W.; Kong, L. The control of epidermal growth factor grafted on mesoporous silica nanoparticles for targeted delivery. *J. Mater. Chem. B* **2015**, *3* (29), 6094−6104.
(19) Williams, N. C.; O' Neill, L. A. J. A Role for the Krebs Cycle Intermediate Citrate in Metabolic Reprogramming in Innate Immunity and Inflammation. *Front. Immunol.* **2018**, *9*, 141.
(20) Wang, F. X.; Prokes, I.; Song, L.; Shi, H.; Sadler, P. J. Reactions of cisplatin and oxaliplatin with penicillin G: implications for drug inactivation and biological activity. *JBIC, J. Biol. Inorg. Chem.* **2022**, *27* (8), 695−704.
(21) Iafisco, M.; Ramírez-Rodríguez, G. B.; Sakhno, Y.; Tampieri, A.; Martra, G.; Gomez-Morales, J.; Delgado-López, J. M. The growth mechanism of apatite nanocrystals assisted by citrate: relevance to bone biomineralization. *CrystEngcomm* **2015**, *17*, 507−511.
(22) Maeda, H. The enhanced permeability and retention (EPR) effect in tumor vasculature: the key role of tumor-selective macromolecular drug targeting. *Adv. Enzyme Regul.* **2001**, *41*, 189−207.
(23) Kuyukina, M. S.; Makarova, M. V.; Pistsova, O. N.; Glebov, G. G.; Osipenko, M. A.; Ivshina, I. B. Exposure to metal nanoparticles changes zeta potentials of Rhodococcus cells. *Heliyon* **2022**, *8* (11), No. e11632.
(24) Altincicek, B.; Shibamiya, A.; Trusheim, H.; Tzima, E.; Niepmann, M.; Linder, D.; Preissner, K. T.; Kanse, S. M. A positively charged cluster in the epidermal growth factor-like domain of Factor VII-activating protease (FSAP) is essential for polyanion binding. *Biochem. J.* **2006**, *394* (3), 687−692.
(25) Clogston, J. D.; Patri, A. K. Zeta potential measurement. *Methods Mol. Biol.* **2011**, *697*, 63−70.
(26) Danaei, M.; Dehghankhold, M.; Ataei, S.; Hasanzadeh Davarani, F.; Javanmard, R.; Dokhani, A.; Khorasani, S.; Mozafari, M. R. Impact of Particle Size and Polydispersity Index on the Clinical Applications of Lipidic Nanocarrier Systems. *Pharmaceutics* **2018**, *10* (2), 57.
(27) Yi, Y. W.; Bae, I. Effects of solvents on in vitro potencies of platinum compounds. *DNA Repair.* **2011**, *10* (11), 1084−1085.
(28) Dasari, S.; Tchounwou, P. B. Cisplatin in cancer therapy: molecular mechanisms of action. *Eur. J. Pharmacol.* **2014**, *740*, 364−378.
(29) Reedijk, J. Increased understanding of platinum anticancer chemistry. *Pure Appl. Chem.* **2011**, *83* (9), 1709−1719.
(30) Jin, S.; Guo, Y.; Guo, Z.; Wang, X. Monofunctional Platinum(II) Anticancer Agents. *Pharmaceutical* **2021**, *14* (2), 133.
(31) Bethune, G.; Bethune, D.; Ridgway, N.; Xu, Z. Epidermal growth factor receptor (EGFR) in lung cancer: an overview and update. *J. Thorac. Dis.* **2010**, *2* (1), 48−51.
(32) Tang, X.; Cheng, L.; Li, G.; Yan, Y. M.; Su, F.; Huang, D. L.; Zhang, S.; Liu, Z.; Qian, M.; Li, J.; Cheng, Y. -X.; Liu, B. A small-molecule compound D6 overcomes EGFR-T790M-mediated resistance in non-small cell lung cancer. *Commun. Biol.* **2021**, *4* (1), 1391.
(33) Ren, J. G.; Seth, P.; Ye, H.; Guo, K.; Hanai, J. I.; Husain, Z.; Sukhatme, V. P. Citrate Suppresses Tumor Growth in Multiple Models through Inhibition of Glycolysis, the Tricarboxylic Acid Cycle and the IGF-1R Pathway. *Sci. Rep.* **2017**, *7* (1), 4537.
(34) Kralj, S.; Rojnik, M.; Kos, J.; Makovec, D. Targeting EGFR-overexpressed A431 cells with EGF-labeled silica-coated magnetic nanoparticles. *J. Nanopart. Res.* **2013**, *15*, 1666.
(35) Bouchard, F.; Bélanger, S. D.; Biron-Pain, K.; St-Pierre, Y. EGR-1 activation by EGF inhibits MMP-9 expression and lymphoma growth. *Blood* **2010**, *116* (5), 759−766.
(36) El-Feky, G. S.; El-Banna, S. T.; El-Bahy, G. S.; Abdelrazek, E. M.; Kamal, M. Alginate coated chitosan nanogel for the controlled topical delivery of Silver sulfadiazine. *Carbohydr. Polym.* **2017**, *177*, 194−202.
(37) Cooper, J. R.; Abdullatif, M. B.; Burnett, E. C.; Kempsell, K. E.; Conforti, F.; Tolley, H.; Collins, J. E.; Davies, D. E. Long Term Culture of the A549 Cancer Cell Line Promotes Multilamellar Body Formation and Differentiation towards an Alveolar Type II Pneumocyte Phenotype. *PLoS One* **2016**, *11* (10), No. e0164438.
(38) Van Meerloo, J.; Kaspers, G. J.; Cloos, J. Cell sensitivity assays: the MTT assay. *Methods Mol. Biol.* **2011**, *731*, 237−245.
(39) Fischer, S. J.; Benson, L. M.; Fauq, A.; Naylor, S.; Windebank, A. J. Cisplatin and dimethyl sulfoxide react to form an adducted compound with reduced cytotoxicity and neurotoxicity. *Neurotoxicology* **2008**, *29* (3), 444−452.
(40) Ghasemi, M.; Turnbull, T.; Sebastian, S.; Kempson, I. The MTT Assay: Utility, Limitations, Pitfalls, and Interpretation in Bulk and Single-Cell Analysis. *Int. J. Mol. Sci.* **2021**, *22* (23), 12827.
(41) Betts-Obregon, B. S.; Vellanki, S.; Buikema, J.; Tsin, A. T.; Wright, K. Effect of Glucose on Retinal Endothelial Cell Viability and VEGF Secretion. *HSOA J. Cell Biol. Cell Metabol.* **2016**, *3* (1), 008.
(42) Kumar, A.; Gatto, G.; Delogu, F.; Pilia, L. DFT study of $[Pt(Cl)_2L]$ complex (L = rubeanic acid) and its derived compounds with DNA purine bases. *Chem. Phys.* **2020**, *530* (110646), 110646.
(43) Barone, V.; Cossi, M.; Tomasi, J. A new definition of cavities for the computation of solvation free energies by the polarizable continuum model. *J. Chem. Phys.* **1997**, *107*, 3210−3221.
(44) Cavasotto, C. N. Binding Free Energy Calculation Using Quantum Mechanics Aimed for Drug Lead Optimization. *Methods Mol. Biol.* **2020**, *2114*, 257−268.

https://doi.org/10.1021/acsomega.3c08969
ACS Omega 2024, 9, 25668−25677